The Magnetosphere Mixing Layer: Observations, MHD Stability, and Large Eddy Simulations

2011 J. Phys.: Conf. Ser. 296 012006

(http://iopscience.iop.org/1742-6596/296/1/012006)

Journal of Physics: Conference Series **296** (2011) 012006 doi:10.1088/1742-6596/296/1/012006

The Magnetosphere Mixing Layer: Observations, MHD Stability, and Large Eddy Simulations

F T Gratton[1,2,5], L E Bilbao[1-3], G Gnavi[1-3] and C J Farrugia[4]

[1] Instituto de Física del Plasma, Consejo Nacional de Investigaciones Científicas y Técnicas y Universidad de Buenos Aires, Buenos Aires, Argentina
[2]- Departamento de Física, Facultad de Ciencias Fisicomatemáticas e Ingeniería, Pontificia Universidad Católica Argentina, Buenos Aires, Argentina
[3] Departamento de Física, Facultad de Ciencias Exactas y Naturales, Universidad de Buenos Aires, Buenos Aires, Argentina.
[4] Space Science Center, University of New Hampshire, Durham, NH, 03824, USA

[5]E-mail: fgratton@arnet.com.ar, fgratton@infip.org

Abstract. The work is about the evolution of large vortices in the boundary layer of the terrestrial magnetopause studied by computational physics, in support of interpretive analysis of spacecraft data from an event observed on December 7, 2000. The distinctive features of the configuration examined are i) the very small magnetic shear across the boundary, and ii) the dynamics concerns mainly the vorticity. The magnetic field is only fluted during the process, but it determines the direction of the vortex axis. Considering new elements from computer simulations and observations, an extension of the research of a recent publication in this journal is reported. A magnetohydrodynamic code for large eddy simulations is used to examine the influence of supersonic, and superAlfvénic speeds, on the dynamics of the boundary layer. Correlations of data are studied to identify signatures of the Kelvin-Helmholtz instability, and the presence of whirling plasma. The aim is to improve the understanding of factors that govern the tailward growth of the low latitude boundary layer, and the potentiality of plasma entry into the magnetosphere, during periods of northward interplanetary magnetic field.

1. Introduction

1.1 Preamble

A short outline of this work is as follows. The stage is the terrestrial magnetopause (MP). We focus the attention on the boundary layer (BL) at the low latitude magnetopause flanks. The paper deals mainly with computational magnetohydrodynamics (MHD) of large vortices. These often form at the BL, and appear more frequently when the interplanetary magnetic field (IMF) shows a significant north component. In addition, we discuss a matter of considerable interest, in view of the scarcity of *in situ* observations. Can records of a single spacecraft that crosses the BL during the transit of quasi-periodic perturbations, pass a judgment of vortex detection? Under what conditions a forecast of the presence of vortices is possible. The paper is a continuation of an investigation recently published in this journal [1] along two directions: *i*) the effect of increasing the magnetosheath flow up to supersonic, and superAlfvénic speeds on vortex simulations, and *ii*) the correlations of experimental data that may disclose the existence of a vortical BL.

1.2 The general context

As appropriate to an introduction, we outline the topic that presently is a cause of concern in magnetospheric physics. This work considers special elements of the larger problem. A cold, dense, magnetized plasma flows around the magnetosphere, gathering speed as it progresses tailward. A tutorial description of the system properties, the global configuration of magnetic fields, and flows can be found, for instance, in [2]. Increasingly, attention has been directed to the presence of magnetosheath plasma deep inside the Earth's plasma sheet when the IMF stays northward for long spells. This plasma is relatively (with respect to ordinary values in the same regions) cold, dense, and stagnant (for example, $T \cong 1$keV, $n \sim 1\text{cm}^{-3}$). See, among other references, [3, 4, 5, 6]. The phenomenon is known as the cold dense plasma sheath (CDPS).

The difficulty is to explain how did this CDPS get there. The presence in the Earth's geomagnetic tail of plasma with properties similar to that of the adjoining magnetosheath makes the flanks a likely entry locale. Indeed, flank entry has often been advocated to explain episodes of CDPS (e.g., [7]). The data records are also well correlated with periods of northward IMF. Hence, the problem is the mechanism of mass entry from solar wind into magnetosphere during northward IMF periods [4, 7].

Two main processes have been suggested. The first one (*a*) is reconnection occurring simultaneously poleward of both cusps. This process adds closed flux tubes filled with magnetosheath plasma to the magnetosphere, into which they slowly sink, as they are convected tailward. See, for instance, [8, 9, 10, 11] and the references quoted in these papers.

The second (*b*) is the velocity shear instability (Kelvin-Helmholtz, KH) in the non-linear stage, when rolled-up vortices that entrain magnetosheath material and broaden the boundary layer are formed. See, [1, 12, 13, 14, 15, 16, 17, 18, 19, 20, 21, 22, 23, 24] and the literature quoted therein. Inside large vortices, the close mingling of magnetosheath with magnetosphere plasma favors the enhancement of particle diffusion at the microscopic scale. Teresawa, Fujimoto, and coworkers (see [4], [7]) pioneered the study of the CDPS formation and the influence of the KH instability on this phenomenon.

Under particular conditions, stretched magnetic field lines may even give rise to small-scale tearing inside a big eddy, and hence to a local de-freezing of plasma and field with consequences on plasma diffusion [12, 13]. However, note that one must distinguish this secondary effect, a consequence of the primary event (the build-up of a KH vortex), from the concept of large-scale reconnection of $\boldsymbol{B}$ field lines poleward of the cusps.

In this paper we consider a different KH scenario, based on a plasma and magnetic field configuration recorded by the Cluster mission during an event of December 7, 2001. The distinctive features are: i) a very small magnetic shear across the boundary, and ii) a dynamics that concerns mainly the vorticity. The process only flutes the magnetic field, although the latter determines the direction of the vortex axis [1, 26, 27]. In another aspect, our simulations differ from other investigations: we use a localized MP model with two free boundaries. We work with two periodicities: along the flow and normal to it (in the sense of the geomagnetic field). The perturbations are free, not anchored, also in the direction normal to the flow.

The two mentioned transfer processes, i.e., (*a*) reconnection poleward of the cusps, and (*b*) KH in its non-linear phase, have been generally considered separately. Several research teams have tried to establish consistency of a small set of observations with models, and simulation ideas of one or other of these two entry mechanisms. These attempts have not yet given a satisfactory elucidation of the issue. It has been shown that one mechanism is more or less sufficient to account for some broad features of the observations in a given case, but it has not been established the necessity by showing the inadequacy of the "*rival*" mechanism in the same situation.

An intrinsic difficulty of the matter of discussion is the dearth of "*in situ*" records. The boundary layer is not observable from afar with other methods, as it happens with several astrophysical systems. For the greatest part one spacecraft alone, if at all, is crossing the MP at interesting times. Moreover, during a spacecraft crossing of the BL it would be desirable to have the support of another in the neighbourhood, to know the state of the magnetosheath at the same time, but this is a rare occurrence.

Hence, the interest to have criteria to identify vortices with data from one spacecraft alone. On the other hand, if available at the proper time and place, the use of multiple spacecraft missions like Cluster and Themis may offer further analysis tools. Thus, for example, some of them might be able, given a favorable satellite constellation, to monitor the magnetosphere and magnetosheath regions adjacent to the vortices. In addition, possibilities of speeds determined by triangulation methods may be feasible.

1.3 The aims of this work

Many aspects of the complex issue just outlined remain obscure, and need further investigations. Considering process (*b*) primary attention should be given to the following factors. The strength and orientation of the magnetosheath's magnetic field, both magnetic and velocity shears across the MP, the flow speed (supersonic, superAlfvénic?), the density gradients across the MP, the scale lengths of the magnetic and velocity transitions (which may be different (e.g., [25, 29]), and the influence of supersonic flows where compressibility, a stabilizing agent, comes into play. When is a flank region KH-stable under supersonic flows? How does the broadening of the flank BL produced by the KH instability depend on (i) the local orientation of ***B*** and ***V***; (ii) the physical conditions at the boundary; and (iii) its distance from the subsolar point? Some of these questions have been addressed by members of our team, and by coworkers in recent studies [1, 23, 24, 26, 27, 28, 29, 30].

On the other hand, the KH instability is associated with other telltale signatures, beside the information provided by "*in situ*" observations. Such are, for example, the geomagnetic micro-

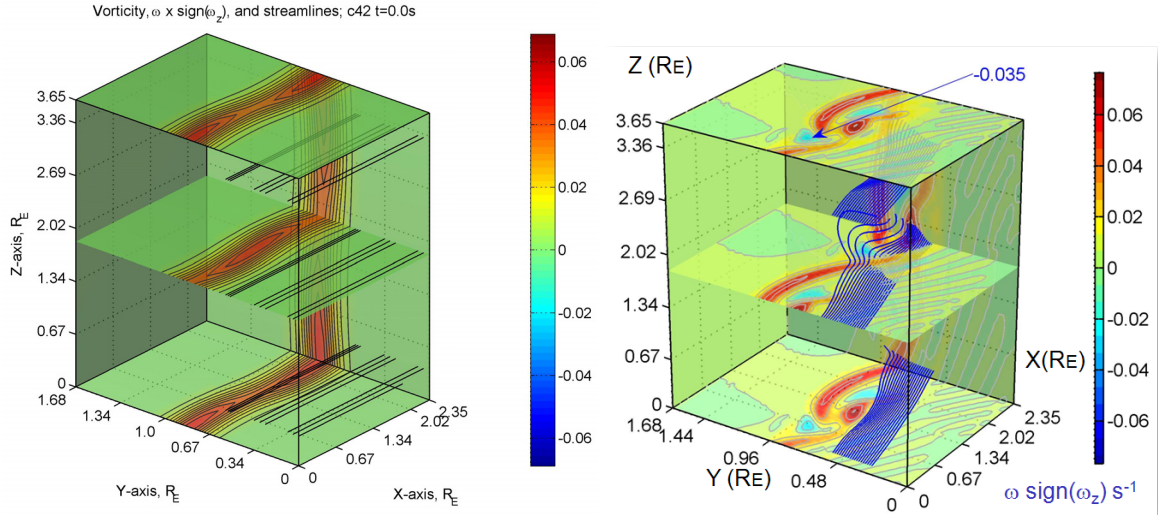

Figure 1a. Left panel. Initial perturbation of the velocity field for the computational run C42. Runs' numbers are explained at the end of Section 2, and their properties are listed in Table 1. Perturbed vorticity contours (color code units s^{-1}) and a set of (black) streamlines on the magnetosheath side. **Figure 1b.** Right panel. LES results for C42 at t=132 s, vorticity contours and a set of (blue) streamlines.

pulsations in the Pc5 range (2-10 mHz). These are quasi-periodic perturbations in the few R_E (Earth radius) wavelength range at the MP flank and BL when the IMF points strongly north. A meaningful example of this phenomenon, with a precise correlation of the frequencies of power spectrum peaks of GOES 8 (Geostationary Operational Environmental Satellites), and of ground magnetometers of the CANOPUS X meridional chain, with the characteristic frequency of the activity observed "*in situ*" by Cluster 3 is reported in [26, 27]. The presence of such signatures constitutes a severe constraint on any interpretation that does not somehow involve the KH instability mechanism.

To recapitulate, (*i*) the rolling-up of the vorticity sheet in the boundary layer must be investigated with compressible, MHD codes. Data analysis and interpretation must be assisted by theoretical and

computational work. Besides, a concurrent theme is (*ii*) to strengthen the knowledge of KH signatures, by making apparent the kind of data correlations that help to diagnose the presence of whirling plasma from *in situ* records of one spacecraft alone. Thus, the paper is oriented toward points (*i*) and (*ii*).

The content of the paper is as follows. After the Introduction, Section 2 summarizes information about December 7, 2000, our KH reference event, and the computational code. Characteristic features of that event are incorporated in the models of the numerical studies. Section 3 presents the main computational results, and their dependence on the sonic, and Alfvén Mach numbers of the magnetosheath flow. Subsection 3.4 focuses on the evolution of strata of different temperature, and density in the BL, and paves the way to Section 4, which deals with the study of correlations of December 7, 2000 data, and their interpretation. Discussion and conclusions are in Section 5.

2. Notes on December 7, 2000, and models for that event

2.1 The reference event

The event that suggests the boundary layer models, the particular disposition of velocity and magnetic fields, and the density and temperature stratifications employed in this paper, is a crossing of the MP recorded by Cluster on December 7, 2000. The phenomenology of this event and the associated theoretical and computational models are given in detail in [1, 26, 27, 29]. Only a minimal description is given here to allow the reader to proceed, skipping a search of references if he/she so prefers.

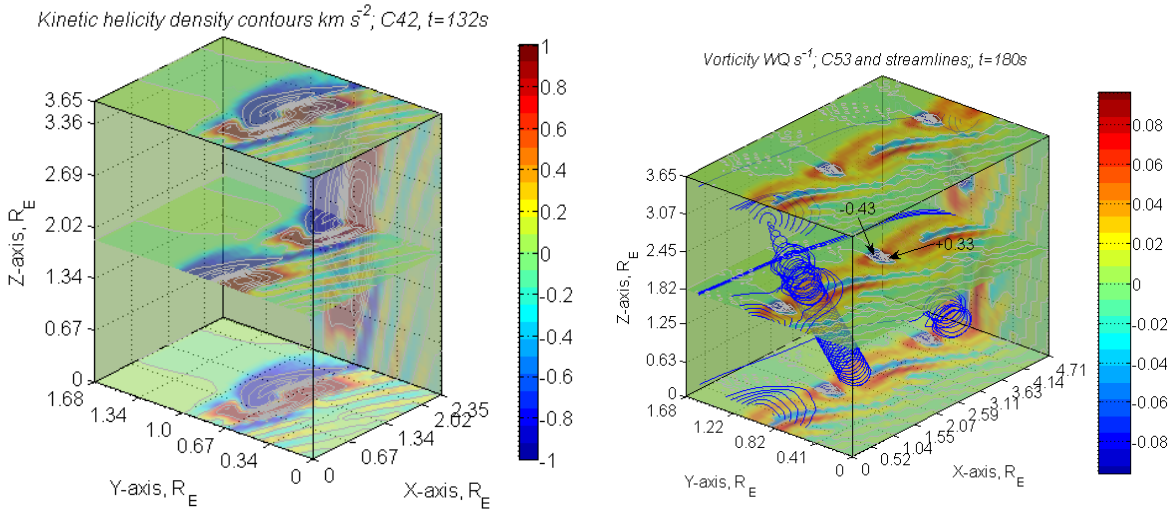

Figure 2 (left). Development of kinetic helicity, C42, t=132 s. The plot show contours of kinetic helicity density $\boldsymbol{V} \bullet \boldsymbol{\omega}$. Note for this and the following figures: we explain runs' numbers, and give their properties at the end of Section 2. **Figure 3 (right).** Details of vorticity evolution for C53 at t=180 s with a view of the distortions of shape of the BL flow and some streamlines of swirling flows.

The period of interest is from 13:55 - 14:28 UT. As can be seen in a plot of Section 4 with plasma data from Cluster 3, the interval is divided in three parts. The first lapse, 13:58 - 14:10 UT corresponds to large amplitude boundary layer oscillations (with a period of about 3 min; 0.050 decimal hours) caused by the impact of a strong solar wind discontinuity onto the MP. The large excursions of the MP are used to obtain an estimate of the speed of the tailward flow of the adjacent magnetosheath, and to gauge the intensity and the change of direction of the magnetic field across the boundary layer, from the inner edge to the magnetosheath [26, 27]. The survey reveals a MP configuration with a very small magnetic shear, and an external flow still subsonic and subAlfvénic.

Monitoring the IMF clock angle with ACE, the permanence of a small magnetic shear angle during the rest of the event can be reasonably assumed. The remaining lapses are then characterized by a very small magnetic shear across the BL. We cannot ensure the outer speed estimate, except as a tentative

evaluation, because of the absence of another spacecraft at the same magnetosheath flank. However, ACE does not register substantial changes of the solar wind speed for the remaining intervals after the first period, which encourages our assumption that the speed estimate holds during the interval of interest. The distinctive aspect of the second and third parts, lasting from 14:10 - 14:28 are quasi-periodic oscillations with a shorter period, 79 s (0.0219 decimal hours). These are strong perturbations of all vector and scalar fields, with intensities decreasing during the third part of the event, from 14:20 to 14:28. After this, a change of the IMF clock angle attested by ACE, determines magnetic conditions unfavorable to the KH instability, and in fact, the former boundary layer activity observed by Cluster 3 extinguishes after 14:28 UT.

2.2 LES and computational code

Eddies generated by the KH mechanism have been extensively studied in fluid dynamics, both with experiments and with numerical simulations. In space physics, the knowledge available on the MHD version of the KH instability has also achieved maturity. In 1984, Miura [31] initiated the computational studies of KH in the MP context. Since then, the steady progress in this area can be appraised in a set of reviews (for instance [32, 33, 34, 14]), and in recent research papers (among others: [1, 12, 13, 15, 16, 17, 18, 19, 20, 22, 23, 24]).

We base the large eddy simulations (LES) on non-dissipative, compressible, MHD equations in 3D and time. The computational program, developed for complex magneto-fluid dynamics problems of plasma physics [37, 38, 39], was adapted for the present task. The in-house code starts from the integral conservation form of the MHD equations, and employs a *finite volume, Lagrangian-Eulerian* technique. The set of equations and some computational features can be found in [1] (this same journal), and more technical details are in [35, 36].

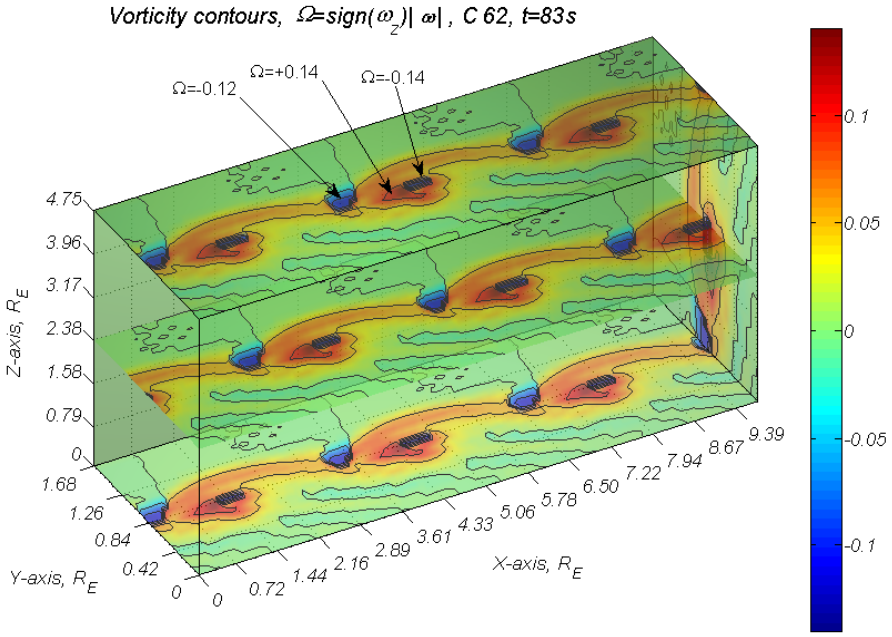

Figure 4. Vorticity contours for C62 at t=83 s. The magnetosheath speed is twice that corresponding to C42, and C53, and the computing box accepts three wavelengths.

2.3 Initial and boundary conditions

Due to the minimal magnetic shear, the MHD theory of the Kelvin-Helmholtz instability predicts significant growth rates for flute modes that have a most favorable angle between the ***k*** – vector and

the direction of the bulk flow at φ=32° [26, 29]. Modes with deviations of $\boldsymbol{k}$ by 10 – 15 degrees from this orientation do not grow. The precise growth rate values depend on the averaged steady state model of fluid and flow employed. We assume hyperbolic tangent functions to connect continuously the vector and scalar fields (magnetic and velocity fields, density and temperature) of the outer magnetosheath limit with those of the inner magnetosphere edge. The same configuration is used as the initial state for the LES, with the addition as initial starter of one perturbation mode only to the velocity field, with amplitudes ranging about 5% the magnetosheath speed. During the simulation, the scalar and vector fields are fixed to constant values as boundary conditions at the outer and the inner limit of the BL.

The computational results are presented in 3D boxes, with the *X*-axis pointing tailward, aligned with the magnetosheath flow, the *Y*-axis is normal to the local part of the MP surface, and points inward across the BL. The *Z*-axis completes a right-hand Cartesian triad (in this case, roughly a north direction). Thus, relative to the BL flow direction, *X* is streamwise, *Y* is transverse (across the flow, pointing into the magnetosphere), and *Z* is spanwise. Note that for LES we chose the positive *X*-axis in a direction contrary to the GSM *x*-axis orientation used in Section 4. Distances along the three axes are in units of the Earth radius (R_E)

The terrestrial MP is perhaps the most important case of *mixing layer* of space physics. In fluid dynamics, a mixing layer is a region between flows of different velocity, often with different density.

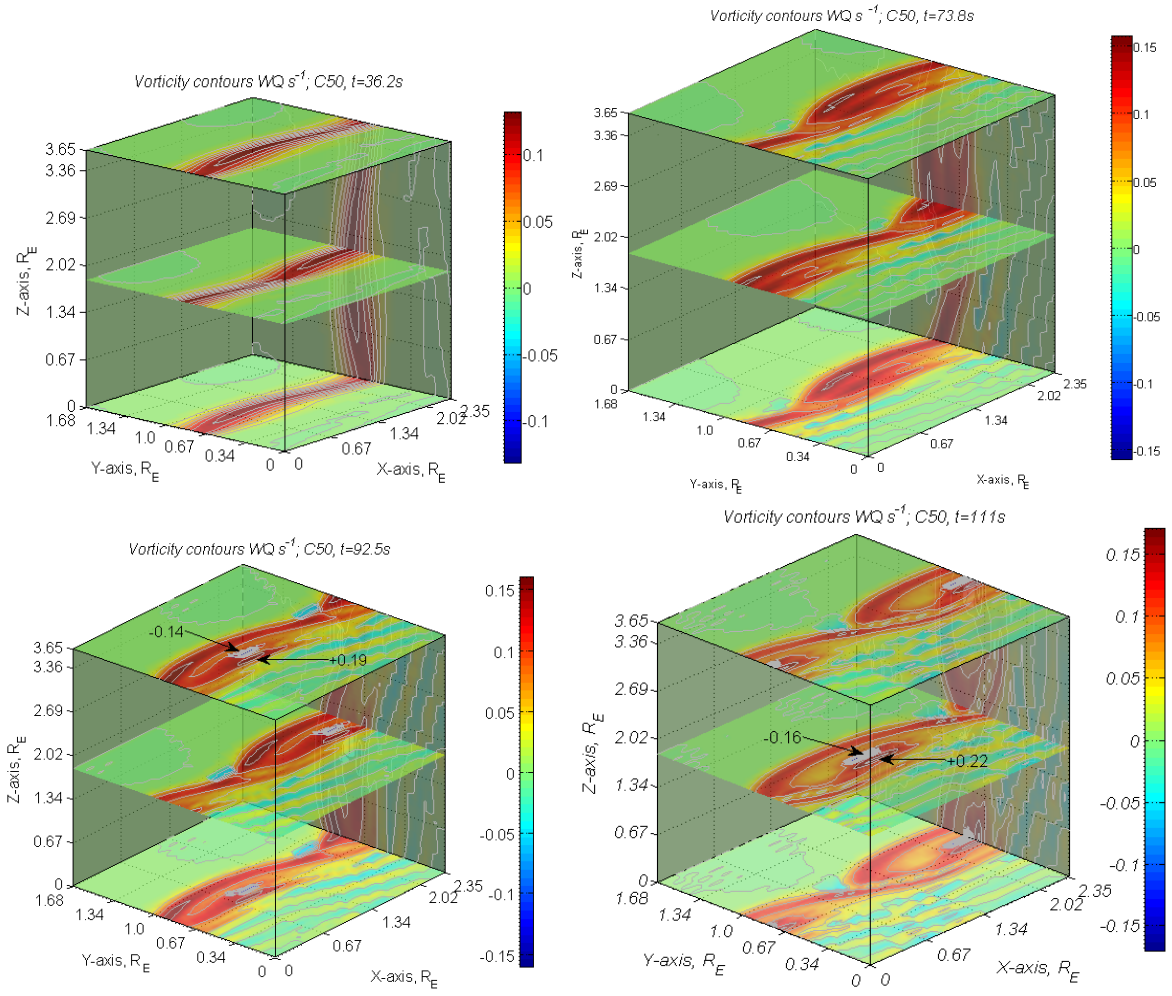

Figure 5. Vorticity rollover for C50, t=36.2, 73.8 (upper panels from left to right), t=92.5, and t=111 (bottom panels from left to right).

In computational fluid dynamics, a *temporal* mixing layer has periodic conditions in the main flow direction (on the box sides' normal to the *X*-axis). The LES of this paper are all of the temporal kind. A difference of our LES with respect to other simulation studies is that we assume periodicity conditions also along the Z-axis, so that perturbations travel freely in a direction that points in the sense of the geomagnetic field.

Unstable temporal mixing layers develop into large vortical patterns, which are called *coherent structures* because they remain for long periods of time, and can be recognized at positions far downstream with approximately similar shapes (see, for instance, [40, 41, 42]).

We compute the non-linear evolution of the KH instability with local BL models that portrait features observed during the Cluster crossing of December 7, 2000 [26, 27]. To investigate the influence of supersonic and superAlfvénic flow regimes on the boundary layer, we then extend the LES to higher magnetosheath speeds, preserving the same configuration of magnetic field, temperature and density boundary values. We also use the LES results to interpret correlations of plasma data measured during the December 7, 2000 event, which reveal the presence of vortical structures that mix magnetosheath and magnetosphere matter.

The computer runs are identified by a number, like C42 that stand for case 42; the number originates from the book-keeping of the physical parameters of particular simulation runs in a large size directory of numerical experiments. The results of only a few computer runs are presented here, and their physical properties are given in Table 1 (at section 3).

3. Computational results: LES dependence on M and M_A

3.1 Vorticity evolution

The initial configuration for the simulations is shown in Figure1a, left panel. The vorticity $\boldsymbol{\omega}$=curl($\boldsymbol{V}$) is represented by the intensity ω=|$\boldsymbol{\omega}$|, to which the sign of the Z component is associated with the formula $\Omega \equiv \omega \times \text{sign}\,(\omega_z)$ s^{-1}. This is because ω_z is the main component that determines the orientation of the vorticity vector. The figure shows vorticity contours Ω associated with the initial perturbation, and a set of streamlines starting at the magnetosheath side of the BL. The computer run is C42, t=0, prepared with one perturbation wavelength that fits into the box, and with the estimated magnetosheath speed for the December 7, 2000 event. The wavevector of the perturbation is set at 32° with respect to the *X*-axis. Only one wavelength fits into the computing box (lengths are in Earth radii, R_E); the *Y*-axis scale length is twice that of the *X*, *Z*-axis to facilitate the view of the MP evolution. The

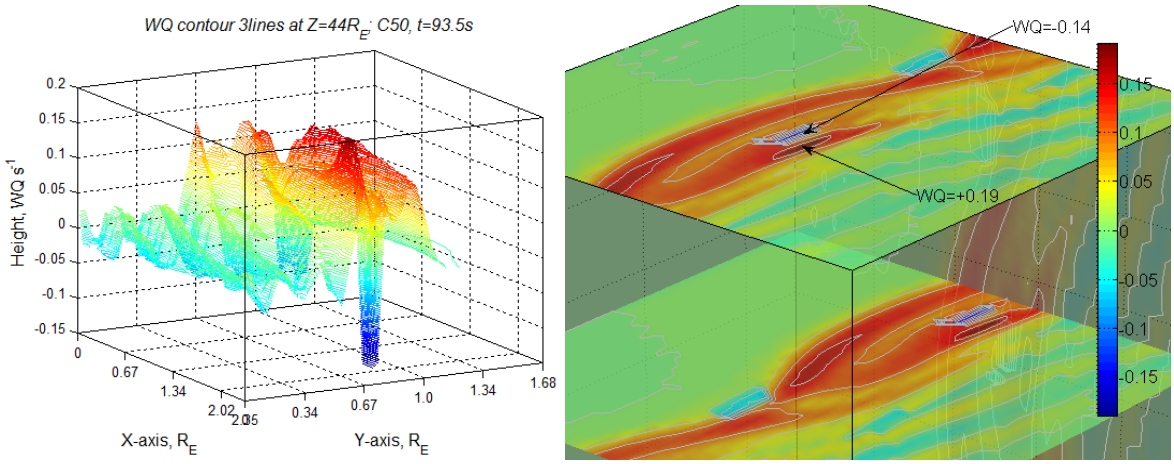

Figure 6. Details of vorticity distribution for C50, t=92.5s. Left panel: vorticity surface on a plane slice Z=44 R_E; the height is $\Omega = \omega \times \text{sign}(\omega_z)$ s^{-1}, and the colors range from red for large positive Ω, to blue for negative Ω. Right panel: a close-up view of Ω vorticity contours, with a color scale.

sonic and Alfvén Mach numbers are M=0.40 and M_A=0.68 respectively, evaluated on the magnetosheath side. The scenario is moderately subsonic and subAlfvénic. Compressibility effects are present but are not strong, as we shall see. The magnetic field, although not visibly affected in shape, because of the quasi-flute arrangement of the fastest growing mode, is nevertheless a dominant factor and influences the topology of the non linear evolution, fixing the orientation of the vortex structures.

In Figure1 b, we show with Ω vorticity contours the evolution of the perturbed vorticity layer after t=132 s, (roughly ¾ of a turnover time for the vortex). Note the concentration of positive vorticity in a vortex core (with intensity amplified by the 3D stretching), and the strained vorticity layer. Two negative vorticity patches have also developed, and are visible at positions of large strain of the shear layer, one closely associated with the positive vortex core. A set of (blue) streamlines, launched from positions near the external side of the boundary layer, are also represented. We observe that the flow is still laminar, but is becoming increasingly 3D at this stage.

The next Figure 2 shows the development of kinetic helicity, for C42, t=132 s, contours of kinetic helicity density $\boldsymbol{V} \bullet \boldsymbol{\omega}$ are displayed. Figure 2 illustrates the progression from the simple, parallel shear flow of Figure 1a, where $\boldsymbol{V} \bullet \boldsymbol{\omega}$ is initially zero, to a complex stage with a large vortex core and deformations of great magnitude of the vorticity layer. Kinetic helicities of both sign arise from the initial velocity field perturbation.

Table 1 summarizes some elements of the computer runs. The case number is in the first column, the second indicates the wavelengths of the initial mode fitted in the computing box. The third column

Table 1. Properties of the simulation cases.

Case	wavelengths	V_1 (km/s)	M	M_A	×
C42	λ	139	0.40	0.68	1
C53	2λ	139	0.40	0.68	1
C62	3λ	278	0.80	1.36	2
C50	λ	420	1.21	2.05	3
C57	2λ	556	1.60	2.72	4

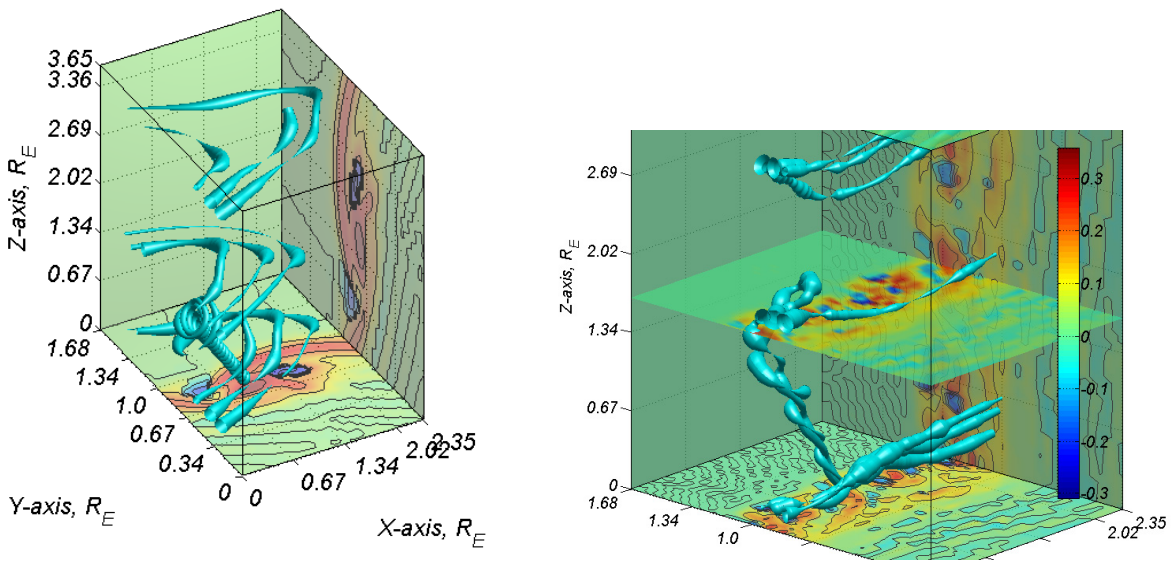

Figure 7 left. Vorticity contours on Z=0, and X=2.35 R_E with stream-tubes, C42, t=132s. The tube section is proportional to div($\boldsymbol{V}$). **Figure 8 right.** Close-up view of vorticity contours and stream-tubes, C50, t=300s; same format as Figure 7

gives V_1 the magnetosheath speed in km/s, and the last column indicates the increased speed factor with respect to the reference case C42. The fourth and fifth columns show the sonic, and Alfvén Mach numbers, respectively.

The Mach numbers, sonic M and Alfvén M_A, of the runs characterize the external magnetosheath flow. Since at the other end, the inner edge of the boundary layer, the magnetosphere velocity is approximately zero, the physical state of motion inside the BL is governed by smaller values of the Mach parameters. This is due not only to the decreasing average velocity in the boundary layer, but also to the increase of temperature, and the diminution of density, as we approach the magnetosphere side. Hence, the sonic Mach decreases in the BL by the action of two causes, the reduction of the average flow velocity, and the increment of the speed of sound. Similarly, the Alfvén Mach number decreases by the diminution of velocity and by the growth of the Alfvén speed due to the smaller density near the magnetosphere side (if the magnetic field intensity remains comparable to the magnetosheath value, as in this case). Therefore, only in the runs with the highest speeds, like the cases C50 and C57, the large outer Mach values begin to exert influence on the physics of the BL. The next vorticity plot, Figure 3, is for C53 at t=180 s (roughly one turn over time). The computer box is prepared to host two wavelengths for the initial perturbation. The plot displays vorticity contours, and shows some streamlines that prove the formation of swirling flows. It shows details of the vorticity evolution, with a close-up view of the distorsions of the boundary layer flow. Note the division of the vortex layer, the warping of the original shape, and the rise of counter-rotating centers.

In Figure 4 , that shows vorticity contours for C62 at t=83 s, the magnetosheath speed is 278 km/s, two times larger than the previous cases C42, and C53. The magnetosheath flow is still subsonic M=0.80, albeit not by a wide margin, and is superAlfvénic M_A=1.36**.** The computing box elongated over the X-axis contains three wavelengths of the initial velocity perturbation. The plot shows the intensification of a row of positive vortices, and their pairing with negative vorticity centers, which are places strongly bent out of shape by the rolling over of the vortex sheet.

In Figures 5 and 6, we examine the process of coupling of vorticity centers of opposite signs at even higher speed. In Figure 5 the rollover of vorticity is for the case C50, in which the magnetosheath speed is 420 km/s (increased three times). It is illustrated by four panels at the times (in seconds) t=36.2, 73.8, 92.5, and t=111 from left to right above, and then again from left to right at the bottom. The external flow is now supersonic, and superAlfvénic, M=1.210, M_A=2.053. The formation of an intense vortex core, and the warping of the initial vorticity sheet are accelerated in this run, and the main features appear earlier. The pairing of large positive and negative vorticity concentrations in small regions is also present, with intensified values. The vortex core is always aligned with the magnetic field direction, as we shall see in other plots.

A closer view on vorticity, for the same case C50 at t=92.5s, is shown in Figure 6. In the left hand side the vorticity distribution on a plane slice, at the position Z=44 R_E of the computing box, is given. The height is $\Omega = \omega \times \mathrm{sign}(\omega_z)$ s^{-1}, and the surface is shaded with colors, red for large positive Ω, down to blue for negative Ω. The positive peak (vorticity amplified by 3D stretching into a strong vortex core) has a close companion, a deep pit of negative vorticity, with a depth in absolute value close to the peak height. The right hand side of Figure 6 shows a close-up of vorticity contours, $\Omega=\omega \times \mathrm{sign}(\omega_z)$ s^{-1}, with a color scale. The close pair of vorticity kernels have Ω=0.19 and Ω=-0.14 s^{-1}.

3.2 Compressibility

We turn now the attention to the effects of compressibility, and the influence of the magnetic field on the mixing layer evolution. Consider again the reference configuration, C42 with 139 km/s as the magnetosheath speed. Figure 7 shows vorticity contours on two sides of the computing box (the bottom Z=0, and the backside X=2.35 R_E) and a set of stream-tubes for t=132s. The tubes are similar to streamlines but with a finite section proportional to div($\boldsymbol{V}$). The stream-tubes are launched at three different heights Z from the plane X=0 (the view is from a reference system moving tailward at half the magnetosheath speed). The tube section is normalized with the initial value at X=0, and the growth or diminution depends on the local value of div($\boldsymbol{V}$). Therefore, the tube section reveals the relative rate

of change of density with time, at each place along the tube. Alternatively, stated with a formula, $\mathrm{div}(\boldsymbol{V})=-(1/\rho)(d\rho/dt)$, where the time derivative is a Lagrangian quantity, i.e., is computed moving along with the flow. Stream-tubes depict graphically the presence of compressibility effects. The figure shows that the boundary layer is, in fact, subject to compressive activity, evidenced by the significant changes of tube sections. Thus even at a subsonic magnetosheath speed, M=0.40 in this case, the rolling-over dynamics, and 3-D stretching, produce important compressive action in the boundary layer.

However, when we examine the stream-tube captured by the vortex, so to speak, which exhibits a swirling pattern, we note that the tube section remains constant as it coils around the vortex axis. We have examined for subsonic magnetosheath flows several other cases, and different times, omitted for brevity. The pattern of compressibility effects is qualitatively similar to that of Figure 7. Thus, for subsonic flows, we can state that during the rollover compressibility effects in the BL are significant, but do not appear to affect the vortex core.

To contrast, Figure 8 gives results of C50 at t=300s to emphasize differences. The speed of the outer flow is increased three times, 420 km/s, and the magnetosheath is supersonic, and superAlfvénic M=1.21, M_A=2.05. With the same format as Figure 7, the plot shows a close-up of stream-tubes. We observe inside the BL, as before, significant Lagrangian changes of density in action. However, now we also note tube section changes of the stream-tube that coils around a vortex. Thus, at the magnetosheath speed level of C50, compressibility has influence also on the vortex kernel dynamics.

3.3 Magnetic field

The magnetic field lines remain straight in all the cases examined. This is due to the small magnetic shear of the field configuration studied here. The fastest growing mode does not bend the magnetic field lines, the perturbations are flute-like, and maintain a flute pattern in the non linear phase. As time goes by, a slight swaying of the magnetic lines can be observed, similar to a wheat field undulating under a light breeze. Nevertheless, the presence of magnetic field is important as it determines the direction of the vortex axis. It also inhibits the development of streamwise vorticity, which is a common feature of ordinary fluid mixing layers. These are the so-called *hairpin* vortices (also known as longitudinal vortices) of the fluid dynamic literature, e.g., [41].

We examine streamwise vorticity with stream-ribbons, as shown in the example of Figure 9. A

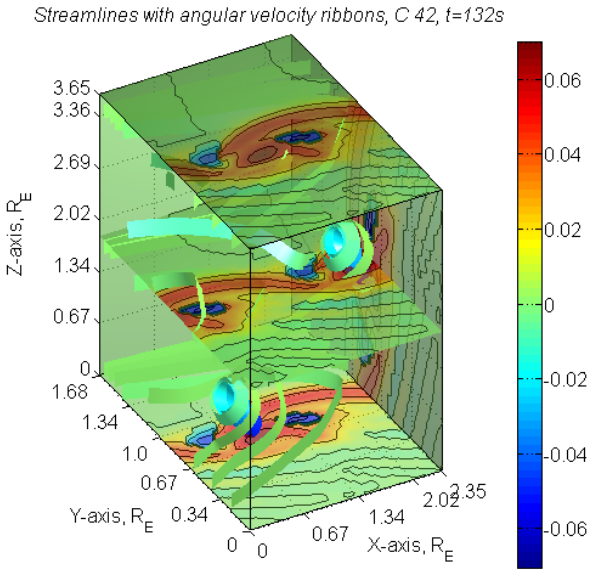

Figure 9. Vorticity contours, and stream-ribbons with twist proportional to |curl(**v**)| for C42, t=132 s.

stream-ribbon is defined like a streamline, with the line replaced by a ribbon of a given width. When there is vorticity along a streamline, the ribbon appears twisted in agreement with the projection of the angular velocity on the line direction. Figure 9 is for C42, t=132 s, it shows vorticity contours, and stream-ribbons where the twist is proportional to |curl(**v**)|. However, the ribbons do not exhibit any worth noting degree of twist, including the ribbon that coils-up around the vortex kernel. We have examined several plots of this kind, always with negative results, reaching the conclusion that the formation of streamwise vortices is absent in our LES. We conjecture that the presence of magnetic field is a hindrance for a process that occurs in ordinary fluids.

Magnetic pressure does not play any noticeable function in the equilibrium of the vortex core in the subsonic cases considered, C42, C53, and C62. However, in supersonic runs, like C57, M=1.60 (fourfold velocity increase) the kernel of largest vorticity becomes also a region of higher magnetic strength. The effect is illustrated in Figure 10 which shows B contours (absolute value of the magnetic field, with a color scale) and a set of magnetic field lines (yellow) for two times. Left panel, t=49s, right panel t=99s. An increase of magnetic field strength in correspondence with vortex loci appears (see also Figure 11), a feature absent in LES at lower speeds.

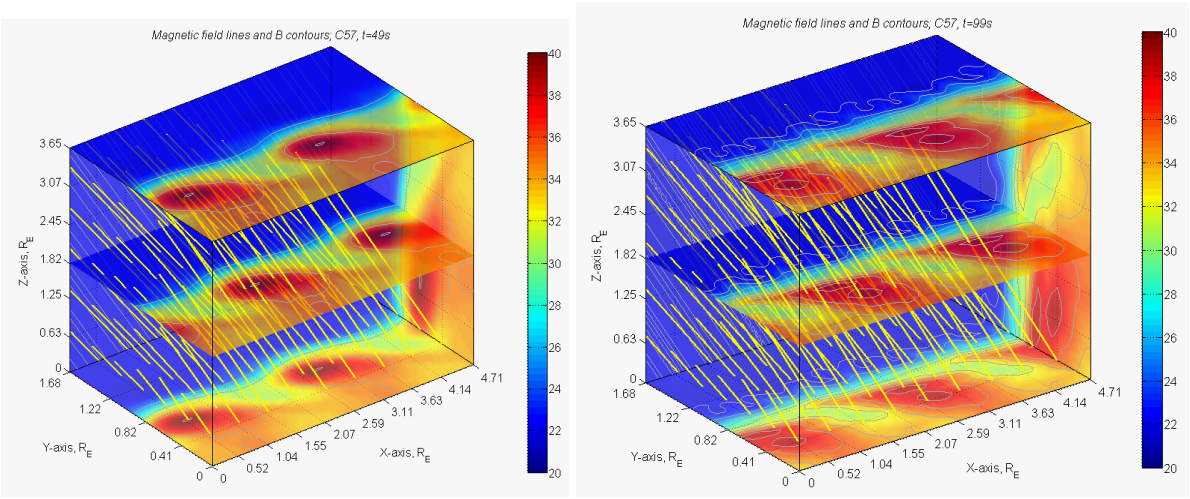

Figure 10. C57, B contours (absolute value of $\boldsymbol{B}$) with a color scale), and magnetic field lines (yellow). Left panel, t=49s; right panel, t=99s.

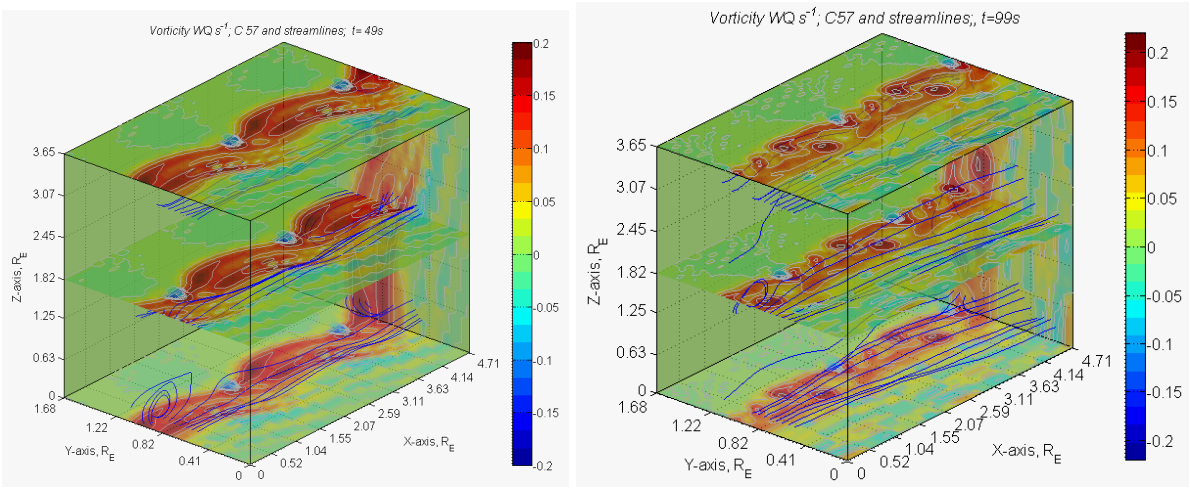

Figure 11. C57 vorticity and streamlines; the left panel is for t=49s, the right panel for t=99s.

Finally, we show, for the same times of Figure 10, the pattern of vorticity contours and some streamlines for C57, the case of greatest speed analyzed. In Figure 11 the left panel is for t=49s, it illustrates the splitting of the vorticity sheet, and the presence of counter-rotating centers. The right panel of Figure 11 is for t=99s, where the pairing of split vortex cores, and the coupling of opposite rotation centers, can be observed. The LES reveals a doubling of positive vortex kernels in the box. A spacecraft in the boundary layer, therefore, should encounter vortices with a twofold increased frequency with respect to the original perturbation.

3.4 Evolution of density and temperature

The vorticity rollover of high speed C50 is examined in Figures 5, and 6. We now consider the mixing of tenuous (closer to magnetosphere values) with dense (nearer to magnetosheath levels) plasma for C50, portrayed in Fig 12 with isodensity surfaces. The time of the run is t=92.5s. Constant (proton) density surfaces for N= 6 (left panel), and N= 11 p cm^{-3} (right panel) are shown. The (blue) velocity cones on the isodensity surfaces indicate the direction of the local velocity field, the size of the cones is proportional to the local speed. The constant density surfaces permit a visualization of vortex tubes, whose inclination is associated with the magnetic field direction. The perspective is rotated around Z, with the Y-axis on the right hand side, for easier visibility of the constant N surfaces.

Details of successive alternations of cold-dense and hot-tenuous portions of matter in the boundary layer can be appreciated in the following two figures. The computer run is C62, with V_1=278km/s, M=0.80 M_A=1.36 (a twofold increase of speed with respect to C42). We plot equal density contours on planar slices at a fixed Z height. Fig 13 shows isodensity contours at two times t=83 s in the upper panel, and t=105 s in bottom right panel. The roll-over is evident, and it is also plain that the density pattern passing over a stationary spacecraft, as the plasma flows downstream, should leave a record of alternate density peaks and valleys, with peculiar shapes that depend on the observation point in the BL, and the evolution time of the vortical structures.

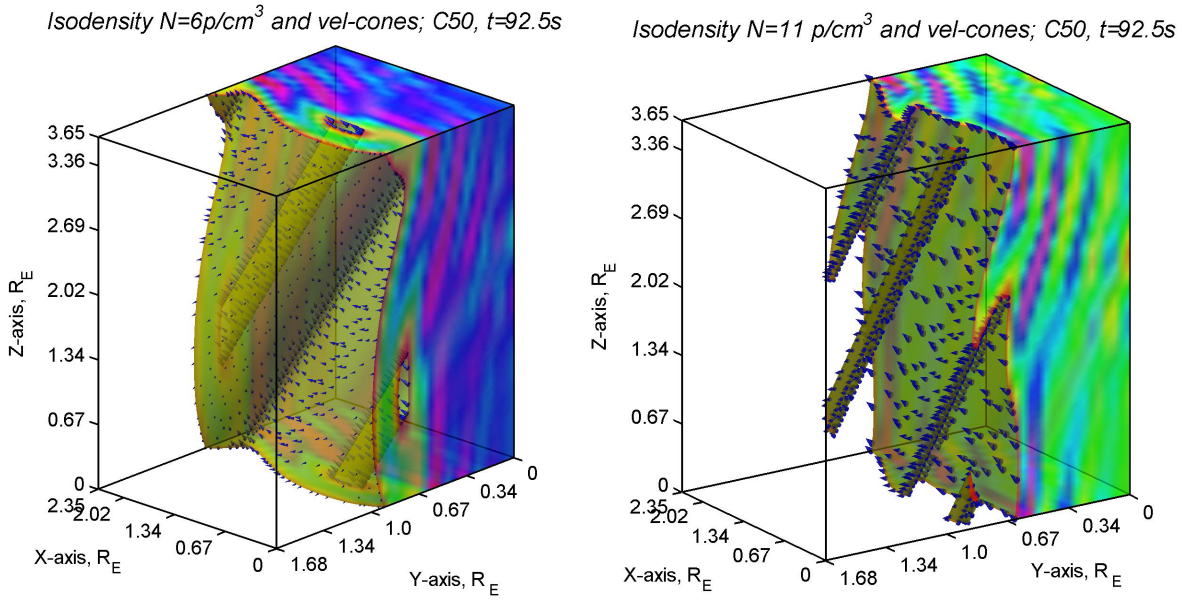

Figure 12. C50, t=92.5s. Constant density surfaces for N= 6, left panel, and N= 11 p cm^{-3}, right panel.

In analogous manner Figure 14 depicts equal temperature contours at a fixed Z plane, at the times 60 s on the left panel, and 105s on the right panel. The alternation of high and low temperatures correlates well with the series of tenuous and dense plasma parts, so that peaks and valleys are always associated in pairs of hot-tenuous and cold-dense sectors. The temperature of C62, at t=105 s, is very

large in certain small parts that coincide with positive vortex kernels, so that the color scale of the plot is set with $ln(T)$. The ratio of the hot spot to the magnetosphere temperature is in the 7 – 8 range.

Therefore, ideal MHD predicts the build-up of vortex cores that are also hot spots. At the moment, it is not clear if the highest temperature value is realistic, or if it exceeds the bounds of our numerical resolution. It remains to be confirmed by future, more elaborated dissipative MHD computations the actual extent of the temperature rise predicted by theory in vortex kernels. In any case, our LES indicate that the trend is there, and it poses a challenge to the ingenuity of the experimentalists to find out whether a significant temperature increment, concentrated in small places of the boundary layer, can be detected by spacecraft instruments.

4. Scatter plots of December 7, 2000 data, and their significance

We show plasma data recorded by Cluster 3 on December 7, 2000 in Figure 15. The plot gives the GSM velocity components versus time, UT, in decimal hours (V_x blue, V_y red, and V_z black lines, km/s). Two other lines are for particle density $N \times 10$ cm^{-3}, green, and temperature T/20 eV, magenta. The event consists of three periods of intense boundary layer activity. The time lapses are associated with changes of the IMF clock angle [26, 27]. The first interval (13.975 - 14.167) shows large amplitude oscillations caused by the arrival of a strong interplanetary perturbation. The following (14.167 - 14.467) two time lapses are interpreted as due to strong (14.167-14.333), and moderate Kelvin-Helmholtz activity (14.333 - 14.467), later quenched by an unfavorable clock angle change of

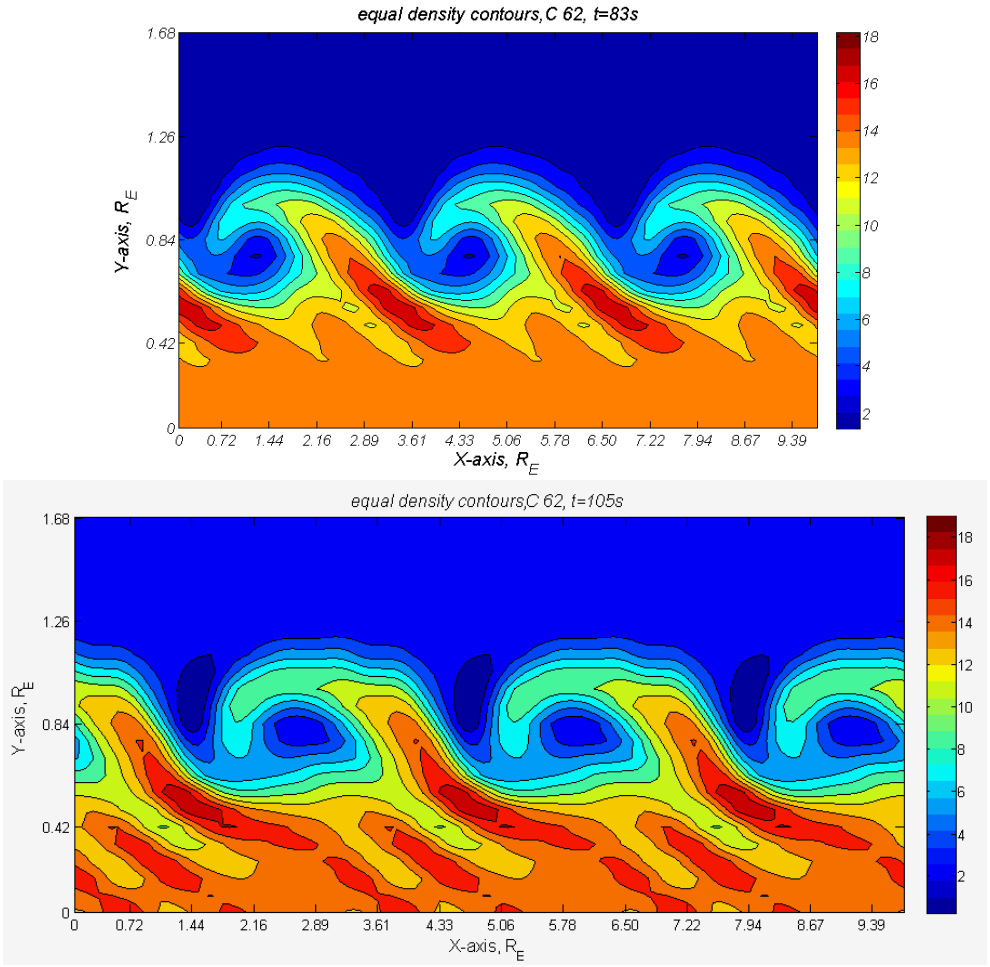

Figure 13. C62, isodensity contours at constant Z; t=83s upper panel, and t=105s bottom panel.

the IMF at the end of the event. The velocity field components (Figure 15) are in the GSM system (Geocentric Solar Magnetospheric [2]), which has its *x*-axis from Earth to the Sun (with the positive sense contrary to the generic magnetosheath flow direction). The *y*-axis is perpendicular to the terrestrial magnetic dipole, pointing to dusk, and *z* is orthogonal to *x*, *y* as in right-hand Cartesian coordinates, so that the *z*-axis is in the same sense as the north magnetic pole.

As can be seen, during the KH interval (14:10-14:28 UT) a principal part of the motion takes place in the *x, y* GSM plane. We therefore associate the *X, Y*, plane of the LES with this plane. The average of measured velocity over the period is $\boldsymbol{V}_{av}$ =(-176.7, 85.1, 28.8) km/s. Note that, V_{yav}, the average of V_y data is not zero, because of the flaring of the magnetopause (the increasing span of the magnetosphere in the anti-sunward direction) at the position of Cluster 3, which estimated from the V_{yav}/V_{xav} ratio is about 26° (where V_{xav} is the corresponding V_x average). Thus, the actual *y*-axis is not normal to the MP, while the simulations assume that *Y* is normal to a MP model. In the following we work mainly with the *x*, *y* velocity components relative to the average, $U_x=V_x-V_{xav}$, $U_y=V_y-V_{yav}$. Hence, we consider the data from a tailward moving frame, with the *y*-flaring effect subtracted. We analyze scatter plots of data to find vortex signatures, i.e., to recognize patterns that herald the presence of whirling matter in the BL. The analysis is on a similar line as [21].

Figure 16 is a scatter plot where the *x* velocity component U_x, and density *N* of each data define a point in the U_x-*N* plane, marked by a circlet. The radius of the small circle is proportional to the

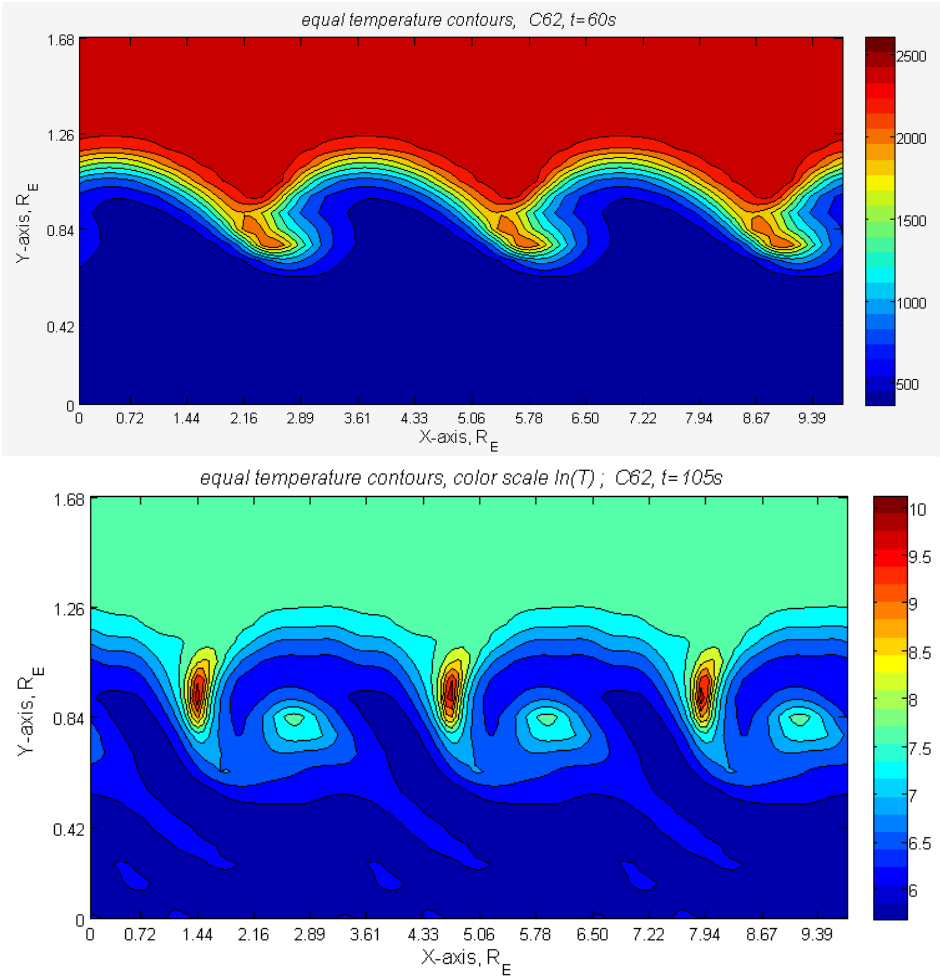

Figure 14. C62, equal temperature contours at constant *Z*; t=60 s upper panel, and t=105s bottom panel with a color scale set with *ln*(*T*).

temperature of the data (larger size corresponds to higher temperature). In addition, to help visibility, we set the color of the marker proportional to $ln(T)$ (red for hot, and blue for cold matter; the logarithm scale is used because of the large range of temperatures).

A linear correlation exists, the majority of low-density plasma moves tailward, and the greater part of high density matter moves sunward. Some tenuous-hot data have very large anti-sunward speeds, and conversely some dense-cold plasma is moving very fast toward the sun.

A scatter plot of temperature, T, versus density, N, is shown in Figure 17. Here the size of the circlets is proportional to $| U_x |$, the absolute value of U_x, i.e., the tailward speed above the average. The color indicates the sign of U_x, red is for sunward and blue for tailward motion. The plot complements the correlation of Figure 16, showing at a glance that a large majority of dense plasma is in motion toward the sun, while on the other hand the greater part of tenuous matter moves anti-sunward. The size shows that there are fast members in both populations. There is a trend from higher to lower temperatures as we shift from lower to higher densities.

Figure 18 is a scatter plot of December 7, 2000, Cluster 3 plasma data. It shows U_y versus U_x (GSM velocity components with average subtracted) where the circlets size is proportional to N^2 (to enhance the tenuous - dense difference), and the color is proportional to $ln(T)$ (red for high temperatures). The time interval is the period of KH activity, 14.167 - 14.467 UT decimal hours (14:20-14:28 UT), when the IMF turns north. The motion is relative to the average of the observed plasma velocity.

The plot shows a linear correlation between $U_x=V_x-V_{xav}$ and $U_y=V_y-V_{yav}$, such that high speed, sunward motions, are predominantly inward oriented (and for the greater part associated with cold-dense plasma). Conversely, fast tailward motions are mainly outward directed (and correspond predominantly to hot-tenuous matter).

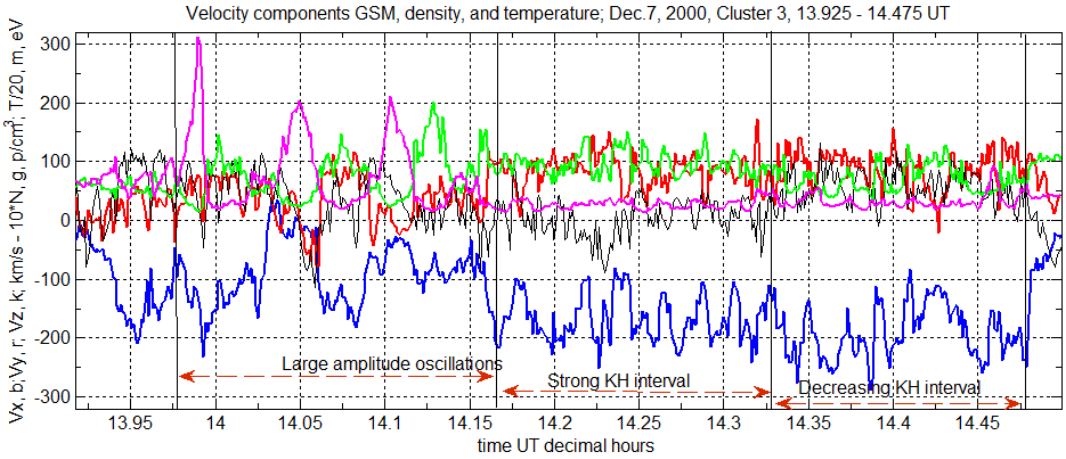

Figure 15. Data recorded by Cluster 3 on December 7, 2000. GSM velocity components versus time, UT in decimal hours (V_x blue, V_y red, and V_z black lines, km/s). The two other lines are for particle density N (scale 10 cm^{-3}), green, and temperature $T/20$ eV, magenta.

The data average of the velocity is the bulk speed of the plasma that passes over the position of the stationary spacecraft (the orbital speed of the device is insignificant compared with that of the plasma). The average is over the KH interval. We have shown with the scatter plots of the BL records, that high temperature, and low-density plasma patches, characteristic of inner layers (close to the magnetosphere) are moving tailward with velocities much higher than the average speed, with increments above average of 50-55 %. On the other hand, cold and high-density plasma, typical of outer strata (close to the magnetosheath), are observed to move sunward, with speeds about 50% higher than the interval average.

Of course, there is also a large set of data values, with intermediate densities and temperatures,

which are moving with velocities close to the bulk plasma speed. However, it is striking and we emphasize the fact, that large velocity differences with respect to the average plasma motion, both in sunward and in tailward directions, are observed during the time lapse associated with the KH instability (due to the negligible magnetic shear). Moreover, we call the attention on the evidence that cold-dense plasma patches are moving sunward, against the magnetosheath flow, with speeds substantially larger than the recorded average, while fractions of tenuous-hot matter move tailward, also with velocities well in excess of the observed average.

Furthermore, because of the U_x-U_y linear correlation, the tailward accelerated hot-tenuous matter moves also predominantly outward (toward the magnetosheath). Conversely, the high speed cold-dense plasma moving sunward also moves mostly inward (toward the magnetosphere). Thus, the scatter plots strongly suggest a composition of plasma motions, i.e., a rotational motion plus a bulk

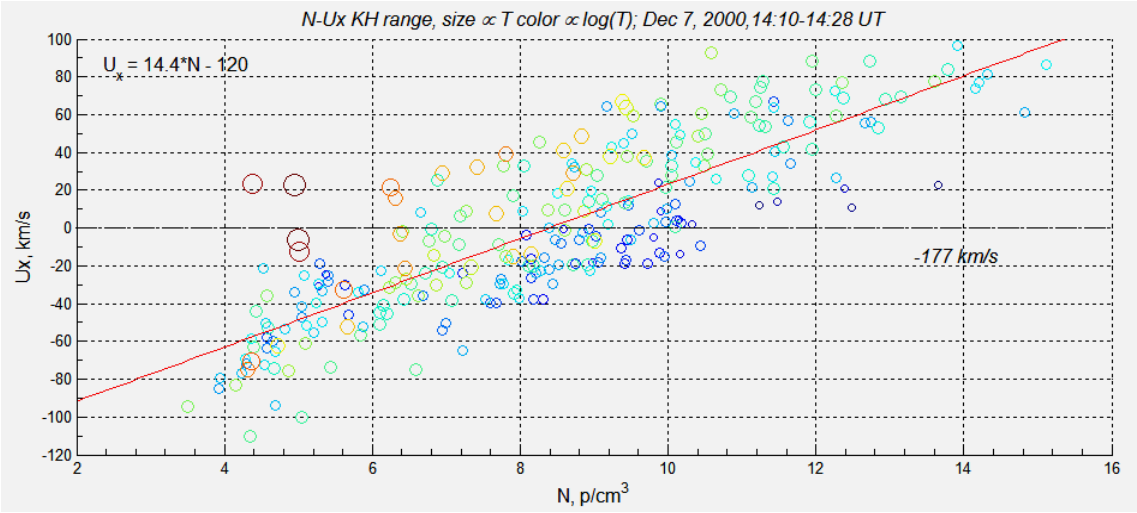

Figure 16. Scatter plot of December 7, 2000 U_x, versus N (data of the KH period). The size of the circlets is proportional to T, the color proportional to $ln(T)$ (see text).

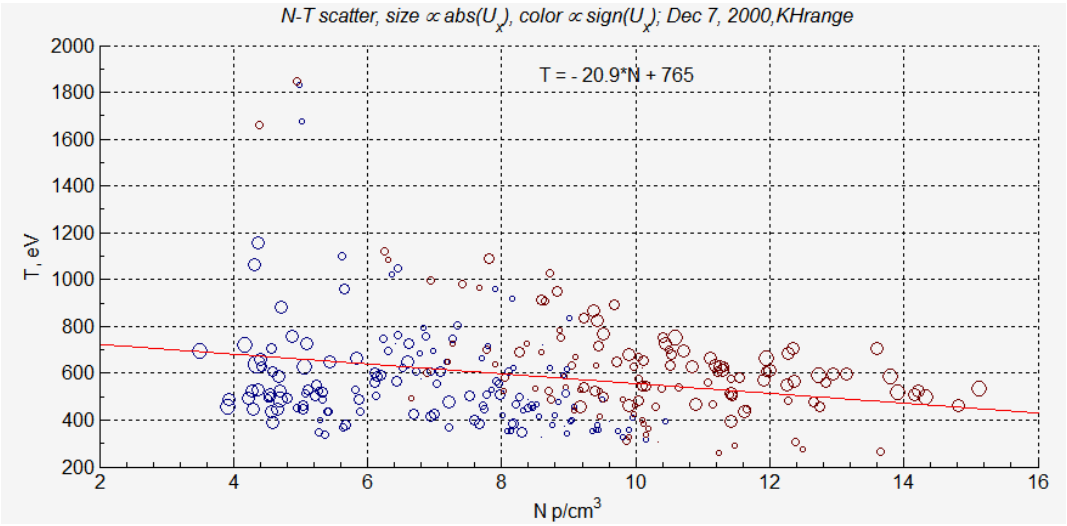

Figure 17. Scatter plot of T versus N. The size of the circlets is proportional to $| U_x |$, the color indicates the sign of U_x (see text).

tailward translation, together with a rolling-over of plasma strata of different density and temperature. In other words, these are the trends qualitatively described by the LES, in subsection 3.4 for example.

Hence, we consider the set of correlations as embodying a criterion that allows, from records of one spacecraft alone, to decide the presence of vortical motions in the BL(on this see also [21]), which therefore becomes an effective mixing layer of inner and outer plasmas.

5. Discussion, summary, and conclusions

It is generally accepted that on time scales much longer than the ion cyclotron gyro-period it is possible to capture the salient macroscopic aspects of the plasma with a theory much more manageable than the kinetic theory of plasmas, which is certainly more fundamental but entails a prohibitive complexity when applied to large-scale phenomena of the interplanetary space.

The theory is MHD, in which the plasma is portrayed as a conducting fluid. In view of the scarce or negligible efficacy of classical Coulomb collisions in interplanetary plasmas, at first sight the use of a fluid model raises some perplexity. However, in space plasmas the relaxation processes are governed by the ubiquitous fluctuations of the electromagnetic field, which produce anomalous transport properties. Particles collide with the fluctuating fields rather than with themselves. The transport problem falls in the realm of plasma turbulence theory, which is the subject of many analytic and numerical investigations. However, while some kinetic theories have attained a highly sophisticated level, the understanding of what happens at the plasma microscale is still modest to be of direct help for large-scale observations. These, on the other hand, are inherently limited by the availability of spacecrafts, and instruments. In practice, the scenarios are so many and so various, that the analysis of many large-scale phenomena, and even some of the meso-scale, are done perforce with macroscopic models.

The MHD equations used in this research are substantially simpler than those of statistical physics. In the decade of 1960, E. N. Parker argued and explained the plausibility of MHD for space physics. Since then, judiciously employed MHD, has been a powerful help in the study of the solar wind dynamics and its interaction with the terrestrial magnetosphere [2]. Of course, due to the non linearity of MHD, mathematical obstacles remain, and due to the manifestations of the subjacent fluctuations, also physical difficulties persist. Nevertheless, in spite of its limitations, the usefulness of MHD for data analysis and interpretation is undeniable. In space physics MHD has not been exhausted, nor superseded.

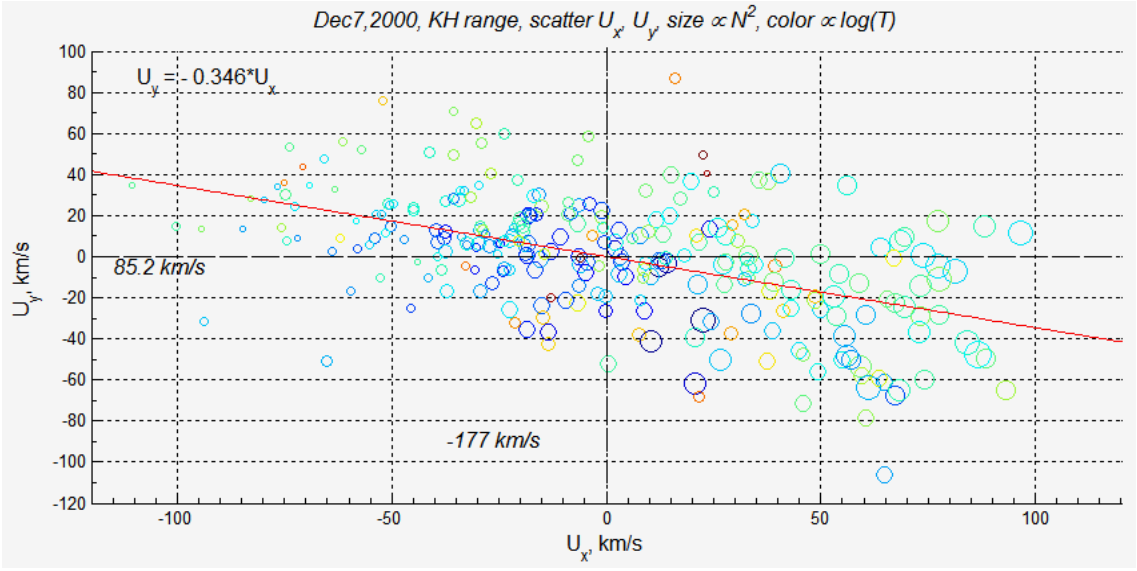

Figure 18. Scatter plot of December 7, 2000 data (KH period) U_y versus U_x. The circlets size is proportional to N^2, and the color is proportional to $ln(T)$.

Moreover, in contrast with what is current in ordinary fluid dynamics, we should recall that the validation of computational and theoretical models in space physics is necessarily indirect and limited. It is often a consequence of the consistent power of the models to explain a variety of different phenomena. Their compatibility with other trusted models or in few special cases their confirmation by a more advanced theory.

The winding-up of the vorticity layer produces large eddies. The 3D vortex stretching intensifies further these structures, as we have seen (also in [1]). The Reynolds number of the large-scale dynamics is given by $R_e = l\mathrm{v}/\nu_{ef}$, where l denotes the vortex diameter, v indicates the rotation speed of the eddy, and ν_{ef} is the effective diffusion coefficient for angular momentum transfer. When the rollover time of the vortex $\tau=l/\mathrm{v}$ is much smaller than the diffusion time, $t_d=l^2/\nu_{ef}$, the Reynolds number is large, $R_e = t_d/\tau >> 1$, a common case in space plasmas. Thus, a range of large-scale lengths can be studied with ideal MHD (ignoring dissipative effects). Dissipative processes become important at much smaller lengths, in the dissipation range where the energy of the eddies finally decays.

Under this condition, the vorticity flux is an invariant of non-stratified fluids, and vortex amplification by 3D stretching then operates with full efficiency. However, although the large-scale dynamics of the eddies can be studied during a few turnover times neglecting dissipation, an advise of caution is in order. In MHD mixing layers the vorticity flux may change with time by causes other than dissipation. The Lorentz force, $\boldsymbol{F}_\mathrm{L}=\boldsymbol{j}\times\boldsymbol{B}/\mathrm{c}$, is in general not ***curl*** free, and $-\nabla\rho\times\boldsymbol{F}_\mathrm{L}/\rho^2$, the associated Lorentz baroclinic term, is not zero either. Moreover, the MP plasma is stratified in a way that the entropy across the BL is not uniform. Thus, in the BL even the ordinary baroclinic term $-\nabla\rho\times\nabla p/\rho^2$ [40] is active. All these causes may affect the invariance of the vorticity flux [1], but it is not clear yet the time scale for the action of these effects in the MP context. In any case, the stretching of vorticity lines occurs in our study, as confirmed by the LES results,

The temporal mixing layer approach is useful and practical, but it has shortcomings. After some periodical returns of the developing vortex into the computing box, the plasma of the actual boundary layer has traveled a distance of many R_E downstream, where the physical conditions in the magnetosheath, and the magnetosphere may have changed, but not so in the LES boundary conditions. Moreover, in the simulations the external magnetosheath flow is assumed laminar, while the solar wind is instead in a fluctuating state, or it is often turbulent. Therefore, the LES presented here are aimed to reveal trends, to foresee global features of the system, but cannot be intended as faithful portraits of observed events.

The paper presents new computational physics, data analysis, and interpretation, associated with a general patterns of fields, and flow, suggested by records of December 7, 2000. This event is taken as representative of a set of low latitude, near flank MPs, with very small magnetic shear under northward pointing IMFs. The near absence of shear of the magnetic field and the flute-like variation of the magnetic lines, during the rollover of the vorticity layer, are characteristic features of the configuration studied. It is the main trait that distinguishes this work from other studies that examine different configurations [12, 13, 14, 15, 16, 17, 18, 19, 20, 21]. The process merely flutes the magnetic field, although the latter determines the direction of the vortex axis [1, 26, 27] and leaves its stamp on the eddies. In another aspect our simulations differ from other investigations: we use a localized MP model with two free boundaries. We have two periodicities: one along the flow, the X-axis, and the other normal to it, the Z-axis that extends in the sense of the terrestrial magnetic field. The dynamics of the perturbations is free also along the Z-axis. The evolution is not restrained by "*ad hoc*" conditions on Z-boundary planes.

The research is a follow-up of [1, 26, 27, 29] that produced original results studying the consequences of increasing the flow speed of the basic configuration .We present new computational plots, and also an analysis of data correlations. The following is a summary of the facts and results obtained, in which we examined the influence of increasing M and M_A in all the points from (a) to (h).

a. Deformation of the vorticity sheet and vortex division; stretching, amplification, and frequency doubling.

b. Generation of swirling flows (initially absent).

c. Development of counter-rotating centers, with associations of positive – negative vorticity kernels.
d. Presence of compressibility effects in the boundary layer, even for subsonic flows. In particular, the vortex core is affected in supersonic but not in subsonic flows.
e. Magnetic "flutes" characterize the configuration; the vortex axis is along the magnetic field; LES show only moderate swaying of the magnetic lines.
f. Evidence of magnetic strength enhancement around vortex kernels in supersonic flows, which is negligible at lower speeds.
g. Mixing of magnetospheric and magnetosheath plasma; alternation of high-low density and low-high temperature strata.
h. Formation of plasma hot spots, i.e., high temperature centers of low density.

In addition, guided by results (f-g) as basic interpretive concepts, we examined scatter plots of velocity, density, and temperature of the reference event data to find signatures of the presence of vortices. Hence, we tested:
i. A criterion to decide the presence of whirling plasma in the BL using records of one spacecraft alone.

To conclude, a brief account of the themes studied in this work is as follows.
1. Large eddy simulations in magnetohydrodinamics set in a counterpoint dialog with the available experimental evidence
2. Understand via computational MHD the physics of stratified and velocity sheared BLs controlled by magnetic fields with negligible change of direction across the MP.
3. Computer simulations of MHD mixing layers, oriented to find trends and to derive guidelines that may help the interpretive effort of MP observations.
4. Analysis of BL data directed to prove the presence of vortical motions with plasma mixing in particular events.

Acknowledgements
Work supported by CONICET grant 11220090100608 PIP 2010 - 2012 ("*La Magnetopausa en Campo Magnético Interplanetario Norte: Análisis de Datos, Teoría y Simulación de Grandes Vórtices*"). Work at University of New Hampshire was supported by NASA grant NNX08AD11G.

References
[1] Gratton F T, Bilbao L E, Farrugia C J and Gnavi G 2009 *JOP Conf. Series* **166** 012023 doi:10.1088/1742-6596/166/1/012023
[2] Russel C T and Kivelson M G eds 1995 *Introduction to Space Physics* Cambridge Un. Press, New York
[3] Fairfield D H, Lepping R P, Hones E W, Bame S J and Asbridge J R 1981 *J. Geophys. Res.* **86** 1396
[4] Terasawa T *et al*. 1997 *Geophys. Res. Lett*. **24** 935
Fujimoto M and Terasawa T 1994*, J. Geophys. Res.* **99** 8601
[5] Fujimoto M, Mukai T and Kokubun S 2002 *Adv. Space Res*. **30** 2279
[6] Øieroset M et al. 2005 *Geophys. Res. Lett.* **32**, L12S07, doi:10.1029/2004GL021523
[7] Fujimoto M *et al.* 1998 *J. Geophys. Res.* **103** 4391
[8] Cowley S W H 1983 in *High Latitude Space Plasma Physics*, ed. Hudqvist B and Hagfors T pp. 225 Plenum New York
[9] Song P and Russell C T 1992 *J. Geophys. Res.* **97** 1411
[10] Raeder J, Walker R J and Ashour-Abdalla M 1995 *Geophys. Res. Lett.* **22** 349
Raeder J et al. 1997 *Geophys. Res. Lett.* **24** 951
[11] Sandholt P E, Farrugia C J, Cowley S W H *et al*. 1999 *Geophys. Res. Lett.* **26** 2833
[12] Otto A and Fairfield D H 2000 *J. Geophys. Res.***105** 21175
[13] Fairfield D H et al. 2000 *J. Geophys. Res.* **105** 21159
[14] Farrugia C J, Gratton F T and Torbert R B 2001 *Space Sci. Rev.* **95** 443

[15] Nykyri K and Otto A 2001 *Geophys. Res. Lett.* **28** 3565
[16] Otto A and K Nykyri K 2003 *Geophys. Monogr.* **133** 53 eds. Newell P T and Onsager T AGU Washington D.C.
[17] Nakamura T K M, Fujimoto M and Otto A 2006 *Geophys. Res. Lett.* **33** L14106 doi:10.1029/2006GL026318
[18] Nakamura T K M, Fujimoto M and Otto A 2008 *J. Geophys. Res.* **113** A09204 doi:10.1029/2007JA012803
[19] Smets R, Delcourt D, Chanteur G and Moore T E 2002 Ann. Geophysicae **20** 757
[20] Hasegawa H, Fujimoto M, Phan T et al. 2004 *Nature* **430**, 755
[21] Hasegawa H, Fujimoto M, Takagi K et al 2006 *J. Geophys. Res.* **111** A09203 doi:10.1029/2006JA011728
Takagi, K., C. Hashimoto, H. Hasegawa, M. Fujimoto, and R. TanDokoro 2006, *J. Geophys. Res., 111*, A08202, doi:10.1029/2006JA011631.
[22] Hasegawa H, Retinò A, Vaivads A et al 2009 *J. Geophys. Res.* **114** A12207 doi: 10.1029/2009JA014042
[23] Gratton F T, Farrugia C J, Bilbao L E, Gnavi G and Lund E 2006 *Am. Inst. of Physics* **C. P. 875** Plasma and Fusion Science pp.300 - 303 ed. Herrera Vázquez J J E Washington DC
[24] Gratton F T, Bender L, Farrugia C J and Gnavi G, 2004 *J. Geophys. Res.*, **109**, A04211 doi:10.1029/2003JA010146
Gratton F T, Gnavi G, Farrugia C J, and Bender L, 2004 *Brazilian J. of Physics*, **34**, 1804
[25] Le G and Russell C T 1994 *Geophys. Res. Lett*. **21** 2451
[26] Farrugia C J, Gratton F T, Lund E J *et al* 2008 *J. Geophys. Res.* **113** A03208 doi:10.1029/2007JA012800
[27] Farrugia C J and Gratton F T 2009 *J. Atmos. Solar-Terr. Phys.* doi:10.1016/j.jastp.2009.10.008
[28] Foullon C, Farrugia C J, Fazakerley A N *et al* 2008 *J. Geophys. Res.***113** A11203 doi:10.1029/2008JA013175.
Foullon C, Farrugia C J, Fazakerley A N *et al* 2010 *J. Geophys. Res.***115** A09203 doi:10.1029/2009JA015189
[29] Gnavi G, Gratton F T, Farrugia C J and Bilbao L E 2009 *J. of Physics* **C.S. 166**, 012022 doi:10.1088/1742-6596/166/1/012023
[30] Farrugia C J, Erkaev N, Torbert R et al. 2010 J. Geophys. Res. **115** A08227 doi:10.1029/2009JA015128
[31] Miura A 1984 *J. Geophys. Res.* **89**, 801
[32] Belmont G and Chanteur G 1989 *Physica Scriptae*, **124** 124
[33] Kivelson M G and Chen S H 1995 in *Physics of the Magnetopause*, Geophys. Monogr. Ser. **90** 257 eds. Song et al AGU Washington, D. C.
[34] Miura A 1995 in *Physics of the Magnetopause*, Geophys. Monogr. Ser. **90**, 285 eds. Song, et al. AGU, Washington DC
[35] Bilbao L E 2006 *Am. Inst. of Physics* **C. P. 875** *Plasma and Fusion Science* pp.467 - 472 ed. Herrera Vázquez J J E Washington DC.
[36] Bilbao L E 2009 *J. of Physics*, **C.S. 166** 012020 doi:10.1088/1742-6596/166/1/012020
[37] Bilbao L E 1990 *J. Computational Physics*, **91**, 361
[38] Bilbao L E and Linhart G 1996 *Plasma Physics Reports* (Fizika Plazmy) **22**, 457
[39] Linhart G and Bilbao L E 2002, *IEEE Trans. Plasma Science*, **30** pp. 460-467
[40] Tritton D J 1988 *Physical Fluid Dynamics*, Clarendon Press, Oxford
[41] Lesieur M 1990 *Turbulence in Fluids*, Kluwer Academic Pub., Dordrecht
[42] Lesieur M and Métais O 1996 *Annual Rev. Fluid Mechanics*, **28** 45.